ACS APPLIED MATERIALS & INTERFACES

Research Article

www.acsami.org

Combined Tween 20-Stabilized Gold Nanoparticles and Reduced Graphite Oxide–Fe_3O_4 Nanoparticle Composites for Rapid and Efficient Removal of Mercury Species from a Complex Matrix

Ya-Chen Shih,[†] Chen-Yi Ke,[†] Cheng-Ju Yu,[†] Chi-Yu Lu,[§] and Wei-Lung Tseng*[,†,‡]

[†]Department of Chemistry, National Sun Yat-sen University, Kaohsiung 804, Taiwan

[‡]School of Pharmacy, College of Pharmacy, Kaohsiung Medical University, Kaohsiung 807, Taiwan

[§]Department of Biochemistry, College of Medicine, Kaohsiung Medical University, Kaohsiung 807, Taiwan

Supporting Information

ABSTRACT: This study describes a simple method for removing mercuric ions (Hg^{2+}) from a high-salt matrix based on the use of Tween-20-stabilized gold nanoparticles (Tween 20-Au NPs) as Hg^{2+} adsorbents and composites of reduced graphite oxide and Fe_3O_4 NPs as NP collectors. Citrate ions adsorbed on the surface of the Tween 20-Au NPs reduced Hg^{2+} to Hg^0, resulting in the deposition of Hg^0 on the surface of the NPs. To circumvent time-consuming centrifugation and transfer steps, the Hg^0-containing gold NPs were collected using reduced graphite oxide–Fe_3O_4 NP composites. Compared with the reported NP-based methods for removing Hg^{2+}, Tween 20-Au NPs offered the rapid (within 30 min), efficient (>99% elimination efficiency), durable (>10 cycles), and selective removal of Hg^{2+}, CH_3Hg^+, and $C_2H_5Hg^+$ in a high-salt matrix without the interference of other metal ions. This was attributed to the fact that the dispersed Tween 20-Au NPs exhibited large surface-area-to-volume ratio to bind Hg^{2+} through Hg^{2+}–Au^+ metallophilic interactions in a high-salt matrix. The formation of graphite oxide sheets and reduced graphite oxide–Fe_3O_4 NP composites was demonstrated using X-ray diffraction, X-ray photoelectron spectroscopy, Raman spectroscopy, Fourier transform infrared spectrometry, and transmission electron microscopy. The mechanism of interaction between Tween 20-Au NPs and Hg^{2+} was studied using visible spectroscopy, transmission electron microscopy, and X-ray photoelectron spectroscopy.

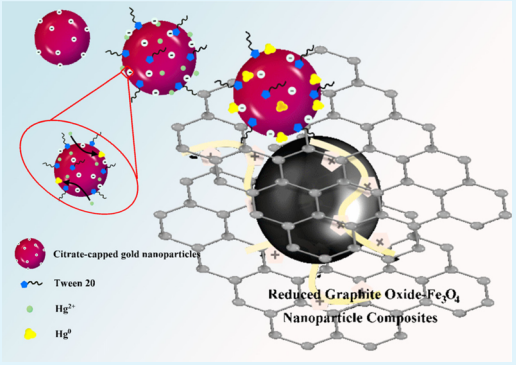

KEYWORDS: *gold nanoparticles, mercury, graphite oxide, Tween 20, Fe_3O_4 nanoparticles, scavenger*

INTRODUCTION

The threat of heavy-metal pollution in water sources is a considerable environmental problem because it causes several adverse health effects. For example, exposure to high levels of mercuric ions (Hg^{2+}) can damage many organs and the immune system.[1] Compared with organic pollutants, non-biodegradable heavy metals can accumulate in living organisms through the food chain. Mercury is one of the most notorious metal pollutants and is widely present in ambient air, water, soil, and even food.[2,3] The maximum level of mercury in drinking water permitted by the U.S. Environmental Protection Agency is 2 ppb (~10 nM). Traditional methods for removing mercury species from nature water and industrial waste include chemical precipitation, ion exchange, amalgamation, electrodeposition, reverse osmosis, photochemical methods, and membrane filtration.[4−9] However, most of these methods are costly, inefficient, and time-consuming. Therefore, numerous solid-phase adsorbents have been developed for the simple, efficient, and cost-effective removal of mercury species by forming Hg–S bonds. Adsorbents include dithizone- and 2-mercaptothiazoline-capped silica gel,[10,11] dimethyl-sulfoxide- and thiosemicarbazide-modified alumina,[12,13] 2-mercaptobenzimidazole-linked agar powder (in a minicolumn),[14] and activated carbon-containing alginate beads.[15] However, these adsorbents exhibit limitations, such as the need for sophisticated synthetic procedures and cross-selectivity toward other heavy metal ions.

Recently, nanomaterials have been introduced to act as adsorbents for the removal of mercury species because they feature a high surface-area-to-volume ratio and are easily chemically functionalized. Additionally, nanomaterials can scan a large volume of solvent in short times because of Brownian motion. Copolymer nanoparticles (NPs),[16] selenium NPs,[17] manganese dioxide nanowhiskers,[18] carbon nanotube–silver NP composites,[19] silver NPs,[20] silver NP-decorated silica spheres,[21] and gold NP-based materials[22−25] were used as scavengers to remove mercury species through a redox reaction, selenium–Hg^{2+} bonding, physisorption, Hg^{2+}–Ag^+ metallophilic interactions, ligand–Hg^{2+} complexation, Hg^{2+}–Ag^+ metallophilic interaction, and Hg^{2+}–Au^+ metallophilic inter-

Received: March 14, 2014
Accepted: September 19, 2014
Published: September 19, 2014

actions, respectively. Among these adsorbents, citrate-capped gold NP-based materials have been used intensively to capture mercury species from nature water. When citrate ions are adsorbed on the surface of gold NPs, the roles of the citrate ions and gold NPs are to act as reducing agents and catalysts in reducing Hg^{2+} to Hg^0.[23] After Hg^0 deposits on the gold surface, Hg^0 diffuses into gold NPs to form a core−shell structure with a gold core surrounded by an Hg−Au amalgam layer.[26] Consequently, citrate-capped gold NPs exhibit a high affinity toward Hg^{2+}, enabling them to serve as effective sorbents for mercury species. However, citrate-capped gold NPs were incapable of efficiently removing mercury species from a high-salt matrix, such as seawater and estuarine water, because citrate-capped gold NPs aggregate in such matrices. In addition, the above-mentioned methods take a long time (hours or days) for the removal of mercury species, need complex synthesis steps, and require additional surface modification.

Nonionic surfactants, including the Tween series (Tween 20, 40, 60, and 80)[27−30] and the Zonyl fluorosurfactant,[31−33] stabilize citrate-capped gold NPs under conditions of high ionic strength and a wide pH range. Moreover, the strong and compact adsorption of nonionic surfactants on the surface of gold NPs efficiently suppress the nonspecific adsorption of macromolecules such as proteins and DNA.[29] Tween 20 behaves as a blocking agent to inhibit nonspecific binding in immunoassays and centrifugal ultrafiltration.[34] Tween 20-stabilized Au NPs (Tween 20-Au NPs) were utilized for sensitive and selective detection of Hg^{2+} under a high-ionic-strength condition (0.1 M NaCl).[30] These results encouraged us to use Tween 20-Au NPs as adsorbents for removing Hg^{2+} from high-salt matrices (seawater and river water). Inductively coupled plasma-mass spectroscopy (ICP-MS) was used to determine the elimination efficiency, while transmission electron microscopy (TEM), X-ray photoelectron spectroscopy (XPS), and absorption spectroscopy were used to verify the presence of Hg^0 in Au NPs. Compared with citrate-capped gold NPs,[23] Tween 20-Au NPs were able to be quick (<30 min), efficient (>99%), selective, and reusable (>10 cycles) to remove organic and inorganic mercury species from a high-salt matrix. To eliminate the time-consuming centrifugation and transfer steps, reduced graphite oxide−Fe_3O_4 NP composites were used to collect the Tween 20-Au NPs from an aqueous solution by applying an external magnetic field.

EXPERIMENTAL SECTION

Chemicals. Hydrogen tetrachloroaurate (III) dihydrate and native graphite flake were purchased from Alfa Aesar (Ward Hill, MA). Trisodium citrate, Tween 20, Na_2HPO_4, Na_3PO_4, NaCl, Na_2SO_4, $MgCl_2$, $CaCl_2$, KCl, $NaHCO_3$, H_3BO_3, $SrCl_2$, NaF, graphite, and poly(diallydimethylammonium chloride) (PDDA; MW 400 000−500 000) were ordered from Sigma-Aldrich (St. Louis, MO). Methylmercury chloride (CH_3HgCl) and ethylmercury chloride (C_2H_5HgCl) were ordered from TCI (Tokyo, Japan). $Hg(ClO_4)_2$, $PbCl_2$, $CrCl_3$, $CuCl_2$, $AgNO_3$, $ZnCl_2$, $CdCl_2$, $FeCl_2$, $FeCl_3$, $AlCl_3$ were obtained from Acros (Geel, Belgium). Water used in all experiments was doubly distilled and purified by Milli-Q system (Millipore, Milford, MA).

Instrumentation. Extinction spectra of gold NPs were recorded using a double-beam UV−visible spectrophotometer (Cintra 10e; GBC, Victoria, Australia). High-resolution transmission electron microscopy (HRTEM, FEI Tecnai G2 F20 S-Twin working at 200 kV) was used to obtain HRTEM images. Energy-dispersive X-ray (EDX) spectra were obtained by combining a scanning electron microscope with an energy-dispersive X-ray detector. The zeta potential of gold NPs was measured using Delsa nano zeta potential and submicrometer particle size analyzer (Beckman Coulter, Inc., Pasadena, CA). The quantification of mercury species in gold NPs was performed by ICP-MS (PerkinElmer-SCIEX, Thornhill, ON, Canada); the linear range for quantification of Hg^{2+} was 2.5−50 nM. Powder X-ray diffraction (XRD) patterns were measured using a diffractometer (model X'Pert Pro; PANalytical, Spectris plc, Almelo, The Netherlands) with Cu Kα radiation. (λ = 1.5418 Å). Magnetometry was performed with superconducting quantum interference device (Quantum Design, San Diego, CA). Fourier-transformed infrared spectroscopy (FT-IR) spectra were measured using a Nicolet 6700 FT-IR spectrometer (Thermo Electron Corporation, Madison, WI).

Preparation of NPs, Buffers, and Stock Solutions. The preparation of citrate-capped gold NPs (10 nM, 13 ± 1 nm) was described in the Supporting Information. The surface-area-to-volume ratio of 13 nm-sized gold NPs is 0.462. The surface area of a single gold NP (13 nm) is 53.2 nm^2. We incubated citrate-capped gold NPs (9 mL, 10 nM) with Tween 20 (1 mL, 10−100% v/v) at ambient temperature overnight. Tween 20-Au NPs (1000 μL) were centrifuged at 14 000 rpm (20 000g) for 20 min. The obtained precipitates were resuspended in 50 μL of deionized water. We stored the as-prepared solution (200 nM Tween 20-Au NPs) at ambient temperature. Tween 20-Au NPs are well-dispersed after 6 months. The cost for 1 mL of 8.3 nM Tween 20-Au NPs is only ca. $0.067. Artificial seawater (salinity 35%) was prepared by dissolving NaCl (23.477 g), $MgCl_2$ (4.981 g), Na_2SO_4 (3.917 g), $CaCl_2$ (1.102 g), KCl (0.664 g), $NaHCO_3$ (0.192 g), KBr (0.096 g), H_3BO_3 (0.026 g), $SrCl_2$ (0.024 g), and NaF (0.003 g) in 1 L of deionized water.[35] Stock solutions of Hg^{2+} (1 mM), CH_3Hg^+ (1 mM), and $C_2H_5Hg^+$ (1 mM) were prepared in deionized water.

Synthesis of Reduced Graphite Oxide−Fe_3O_4 NPs Composites. Synthesis of graphite oxide was performed according to Hummer's method.[36] Briefly, we treated native graphite flake (1 g) with a solution of concentrated H_2SO_4 (1.5 mL) containing $K_2S_2O_8$ (0.5 g) and P_2O_5 (0.5 g) and incubated them at 80 °C for 6 h. The product was washed with deionized water until the rinsewater was neutral. The obtained preoxidized graphite was then dried in air at ambient temperature. The preoxidized graphite (1 g) was immersed in concentrated H_2SO_4 (23 mL) at 0 °C. Subsequently, $KMnO_4$ (3 g) was gradually added into the mixture with stirring while maintaining the reaction temperature below 20 °C. The obtained mixture was further stirred at 35 °C for 2 h, followed by the addition of deionized water (46 mL). After 15 min, the reaction was terminated by adding deionized water (140 mL). After adding 30% H_2O_2, the color of the resulting solution turned bright yellow. The resulting solution was centrifuged and washed with HCl (250 mL, 10%) to remove residual metal and SO_4^{2-} ions. The obtained precipitate was washed with deionized water and centrifuged repeatedly until the rinsewater was neutral. Exfoliation of the product was achieved under the treatment of ultrasound sonication (Elma, South Orange, NJ; 150 W, 135 kHz) for 30 min. This treatment enables graphite oxide to be dispersed in deionized water. We denote the concentration of the as-prepared exfoliated graphite oxide as 1.0×.

To synthesize reduced graphite oxide−Fe_3O_4 NP composites, graphite oxide (10 mL, 0.1×) was incubated with PDDA (10 mL, 2% v/v) at ambient temperature for 1 h. The PDDA-coated graphite oxide was mixed with $FeCl_3{\cdot}6H_2O$ (2.16 g) and $FeCl_2{\cdot}4H_2O$ (0.8 g); the resulting solution was deoxygenated by bubbling with nitrogen gas for 10 min, followed by heating to 80 °C for 10 min. NH_4OH (10 mL, 8 M) was added rapidly to the heating solution which was left to stir for 1 h. After cooling to ambient temperature, the formed reduced graphite oxide−Fe_3O_4 NP composites were magnetically collected, washed two times with deionized water (100 mL), and dried at 80 °C. The collected composites were weighed using an analytical balance. The concentration of reduced graphite oxide−Fe_3O_4 NP composites was estimated to be 12.2 mg/mL.

Removal of Mercury Species. Tween 20-Au NPs (50 μL, 200−1000 nM) and citrate-capped gold NPs (50 μL, 200 nM) were separately incubated with a solution (1150 μL) containing mercury species (Hg^{2+}, CH_3Hg^+, and $C_2H_5Hg^+$; 120 μL, 10−1000 μM) and artificial seawater (1030 μL) at ambient temperature for 0−24 h.

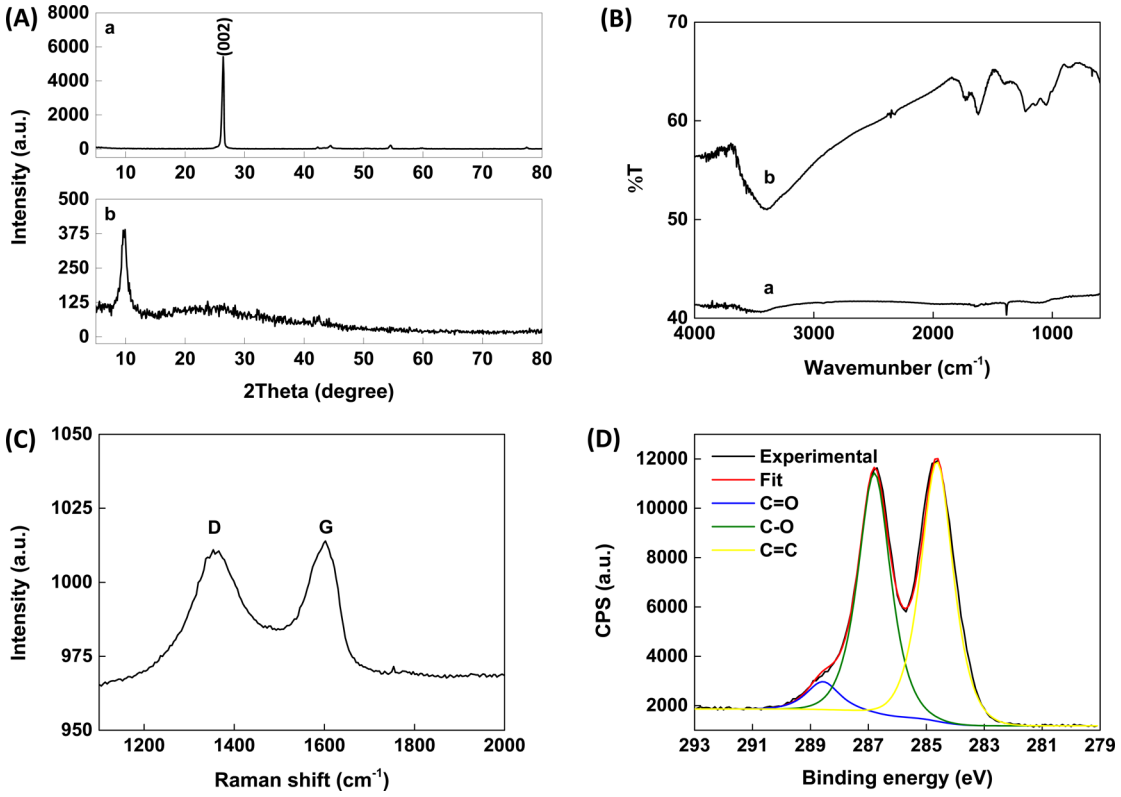

Figure 1. (A) XRD and (B) FT-IR spectra of (a) graphite and (b) graphite oxide. (C) Raman and (D) XPS spectra of graphite oxide.

Caution: Because CH_3Hg^+ and $C_2H_5Hg^+$ are highly toxic and volatile, it is strongly recommended that work take place in an appropriate fume hood.

By applying an external magnetic field, reduced graphite oxide–Fe_3O_4 NP composites (8.3 mg/mL) were used to collect Tween 20-Au NPs or citrate-capped gold NPs from an aqueous solution. The quantification of Hg^{2+} in supernatant was determined by ICP-MS. Elimination efficiency was calculated as the following:

$$\text{Elimination efficiency}\ (\%) = [(C_0 - C)/C_0] \times 100$$

where C_0 is the initial concentration of Hg^{2+} and C is the final concentration of Hg^{2+} in the supernatant. The equilibrium adsorption capacity was determined according to the following equation:

$$q_e = (C_0 - C_e) \times (V/W)$$

where q_e (mg of Hg^{2+}/g of nanoparticles) is the equilibrium adsorption capacity, C_e is the Hg^{2+} concentration at equilibrium, V is the volume of solution, and W is the weight of Tween 20-Au NPs.

To demonstrate the selectivity of Tween 20-Au NPs, we used other metal ions in place of mercury species. To test the reusability of Tween 20-Au NPs, we heated a mixture of Hg^{2+}-adsorbed gold NPs and reduced graphite oxide–Fe_3O_4 NP composites to 30–80 °C for 10 min. The heat-treated composites (50 μL) were incubated with Hg^{2+} (1150 μL, 10 μM) at ambient temperature for 30 min. After we collected the composites by applying an external magnetic field, we determined the concentration of Hg^{2+} in supernatant by ICP-MS. This procedure was repeated 18 times to determine the reusability of the proposed method.

Samples of river water and seawater were collected from the Love River in the Kaohsiung City and from the Siziwan Bay on the National Sun Yat-sen University campus. We then prepared a series of samples by spiking river water and seawater samples (1030 μL) with Hg^{2+} (120 μL, 150 μM). The resulting solutions were incubated with Tween 20-Au NPs (50 μL, 200 nM) at ambient temperature for 30 min. The following steps, including the collection of Tween 20-Au NPs and ICP-MS analysis, were the same as those used in the determination of removal efficiency of Hg^{2+} in artificial seawater.

RESULTS AND DISCUSSION

Characterization of Reduced Graphite Oxide–Fe_3O_4 Nanoparticle Composites. To demonstrate the formation of graphite oxide, we examined the products prepared from Hummer's method[36] using XRD, FT-IR, Raman, and XPS spectroscopy. After the graphite was strongly oxidized, the sharp and intense (002) peak of graphite at 27° disappeared, and a broad peak appeared at 10° (Figure 1A). This shift indicates the production of graphite oxide, which is consistent with previous XRD measurement of graphite oxide.[37,38] The FT-IR spectrum of graphite shows no functional group on the surface (curve a in Figure 1B). By contrast, the FT-IR spectrum of the produced graphite oxide exhibited three major bands at 1622, 1737, and 3391 cm^{-1} (Curve b in Figure 1B), which arise from the stretching vibrations of C═C, C═O, and O–H, respectively. This result indicates that the graphite oxide contained carboxyl and hydroxyl functional groups. Previous studies have reported the same features.[38,39] The Raman spectrum of the graphite oxide reveals that the intensity ratio of the D band to the G band was approximately 1.0 (Figure 1C), signifying the presence of oxygen-related functional groups such as hydroxyl and carboxyl groups.[40,41] Figure 1D shows a deconvoluted C_{1s} XPS spectrum of the dried graphite oxide. The peaks at 284.6, 286.7, and 288.6 eV arose from C═C, C–O, and C═O, respectively, confirming the presence of oxygen-containing functional groups.[42]

Adding 1% v/v PDDA to a solution of graphite oxides caused electrostatic repulsion between the graphite oxides, preventing them from aggregating in water.[43] This is attributed to the fact that positively charged PDDA exhibits a strong electrostatic

dx.doi.org/10.1021/am5033988 | ACS Appl. Mater. Interfaces 2014, 6, 17437–17445

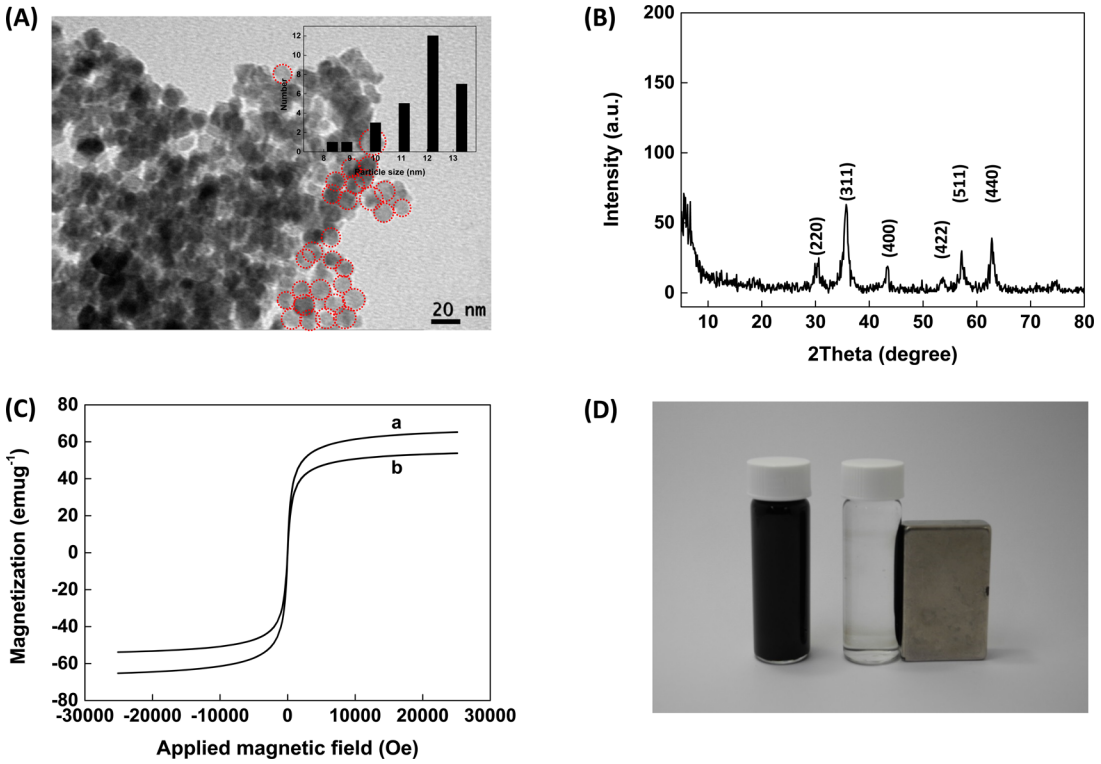

Figure 2. (A) TEM image and (B) XRD spectrum of reduced graphite oxide–Fe_3O_4 NP composites. The red circles in part A indicate Fe_3O_4 NPs. (C) Room temperature magnetization curves of (a) Fe_3O_4 NPs and (b) reduced graphite oxide–Fe_3O_4 NP composites. (D) Picture of a solution of reduced graphite oxide–Fe_3O_4 NP composites under the effect of a permanent magnet.

attraction toward negatively charged graphite oxide. The composites were synthesized through a one-step hydrothermal reaction of Fe^{3+}, Fe^{2+}, and PDDA-coated graphite oxide in the presence of NH_4OH. Figure 2A depicts a TEM image of the as-prepared hybrid, in which Fe_3O_4 NPs were spherical and had an average diameter of 12 ± 1 nm. Obviously, adding PDDA-coated graphite oxide to a precursor solution did not impede the formation of Fe_3O_4 NPs. The XRD spectrum of the as-prepared hybrid exhibited diffraction peaks at 2θ = 30.3°, 35.7°, 43.2°, 53.3°, 56.9°, and 62.5°, corresponding to the (220), (311), (400), (422), (511), and (440) planes of the face-centered cubic lattice of Fe_3O_4, respectively (Figure 2B). These characteristic peaks reflected that the reaction for generating Fe_3O_4 NPs still proceeded in the presence of the PDDA-coated graphite oxide. However, the broad peak of graphite oxide at 10° was not observed in the XRD spectrum of the as-prepared composites. This could be attributed to PDDA-induced deoxygenation of graphite oxide, resulting in the formation of reduced graphite oxide.[43] The magnetic properties of the Fe_3O_4 NPs and the resultant composites were investigated using a superconducting quantum interference device magnetometer at room temperature. The saturation magnetizations of the Fe_3O_4 NPs and the resultant composites were 65.2 and 53.8 emu/g, respectively (Figure 2C). The magnetization versus magnetic field measurement at 300 K for the two types of nanomaterials exhibited zero coercivity and remanence, indicating that the materials were superparamagnetic. Compared to the Fe_3O_4 NPs, a 14% decrease in saturation magnetization of the resultant composites could be attributed to the contribution of the overall mass from nonmagnetic PDDA-coated reduced graphite oxide. This result also indicates that 1 g of composites consists of 0.14 g reduced graphite oxide and 0.86 g Fe_3O_4 NPs. When the saturation magnetization is higher than 16.3 emu/g,[44] a magnet can be used to separate a magnetic material from a solution. Thus, Figure 2D shows that the resultant hybrid quickly moved to the sidewall of the vial when exposed to a bar magnet.

Using Tween 20-Au Nanoparticles Coupled to Reduced Graphite Oxide–Fe_3O_4 Nanoparticle Composites to Remove Mercury Species. Reduced graphite oxide–Fe_3O_4 NP composites were tested to collect Tween 20-Au NPs from artificial seawater. We propose that the role of reduced graphite oxides in composites is to act as an adsorbent for Tween 20-Au NPs via van der Waals interaction. Moreover, Fe_3O_4 NPs in composites are used as a magnetic carrier. Likewise, Jeon and Lee demonstrated that negatively charged Au NPs were capable of attaching onto the surface of graphene sheet.[45] XPS was utilized to prove this hypothesis. Figure S1 (Supporting Information) shows that the collection of Tween 20-Au NPs with reduced graphite oxide–Fe_3O_4 NP composites resulted in two binding-energy peaks at 87.5 and 83.8 eV, which were assigned to Au $4f_{5/2}$ and Au $4f_{7/2}$, respectively. Apparently, reduced graphite oxide–Fe_3O_4 NP composites indeed captured Tween 20-Au NPs in artificial seawater. The zeta potential of Tween 20-Au NPs was measured to be −5.5 ± 0.8 mV in artificial seawater, signifying that the presence of salt and Tween 20 almost neutralizes the surface charge of citrate-capped gold NPs. However, Tween 20-Au NPs were still dispersed in artificial seawater because of the steric hindrance of Tween 20. We tested the ability of Tween 20-Au NPs to remove Hg^{2+} from artificial seawater. The as-prepared artificial seawater contains a high concentration of NaCl, indicating that $HgCl_2$ complexes exist in artificial seawater. Tween 20-Au NPs (8.3 nM) were incubated with 1.2 mL of 10 μM (2 ppm) Hg^{2+}

dx.doi.org/10.1021/am5033988 | ACS Appl. Mater. Interfaces 2014, 6, 17437−17445

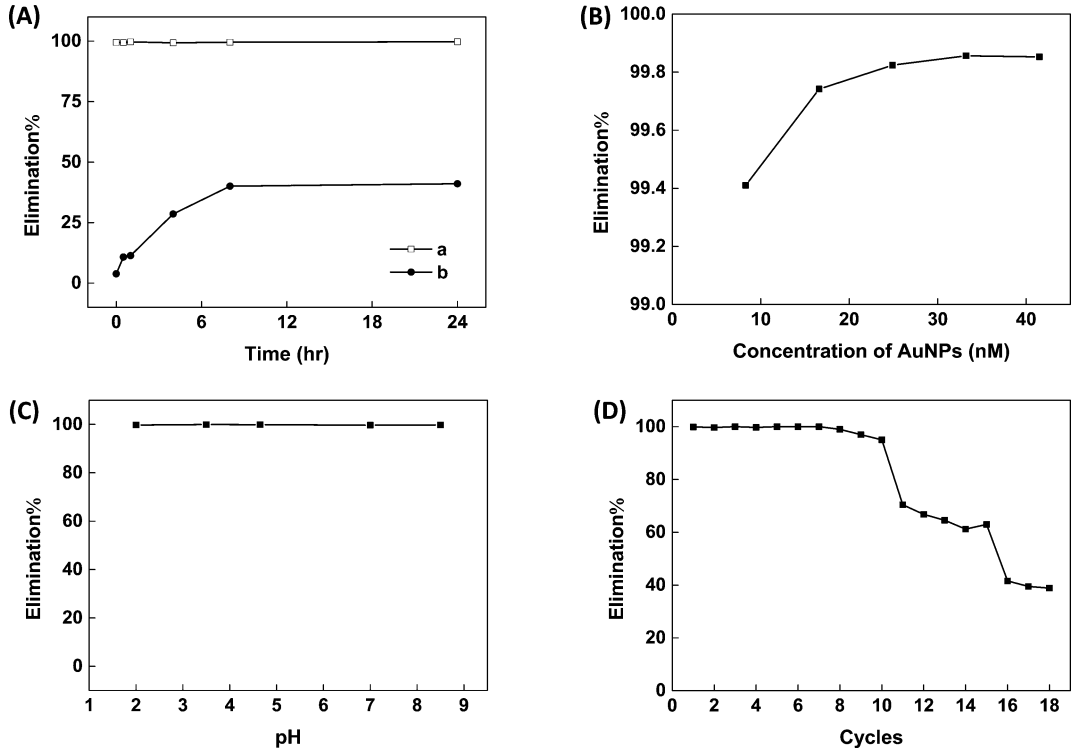

Figure 3. (A) Effect of incubation time between (a) 10 μM Hg^{2+} and 8.3 nM Tween 20-Au NPs and (b) 10 μM Hg^{2+} and 8.3 nM citrate-capped gold NPs on the elimination efficiency. (B) Effect of the concentration of Tween 20-Au NPs on the elimination efficiency of 10 μM Hg^{2+}. The incubation time is 30 min. (C) Effect of the solution pH on the elimination efficiency; 10 μM Hg^{2+} was incubated with 8.3 nM Tween 20-Au NPs for 30 min. (D) Elimination efficiency of 10 μM Hg^{2+} in recycle runs using regenerated and reactivated gold NPs (8.3 nM). The incubation time is 30 min in each cycle.

at ambient temperature for 0−24 h. ICP-MS was used to determine the concentration of Hg^{2+} in the supernatant at various incubation times because of its high selectivity and sensitivity for Hg^{2+}. Note that ICP-MS was capable of detecting Hg^{2+} concentrations as low as 250 pM. Tween 20-Au NPs removed >99.3% of the 10 μM Hg^{2+} within 30 min (Curve a in Figure 3A). By contrast, citrate-capped gold NPs removed only 41% of the 10 μM Hg^{2+} by 24 h (Curve b in Figure 3A). Because salts induce citrate-capped gold NPs to aggregate (Figure S2, Supporting Information), a decrease in the surface-area-to-volume ratio leads to a decrease in the elimination efficiency. However, Tween 20-Au NPs were stable in artificial seawater (Figure S3, Supporting Information), enabling them to efficiently capture Hg^{2+}. Puntes et al. reported that citrate-capped gold NPs (6.6 nM) removed 58% of 24 μM Hg^{2+} in deionized water.[23] Liu et al. used DNA-functionalized hydrogels to capture 97% of 1 μM Hg^{2+} in deionized water by 6 h.[46] Compared with the adsorbents used in previous studies,[23,46] Tween 20-Au NPs provided the advantages of rapidity, simplicity, and efficiency for removing Hg^{2+} from high-salt matrices. The maximum elimination efficiency of Hg^{2+} was examined by varying the concentration of Tween 20-Au NPs at a fixed concentration of Hg^{2+}. The elimination efficiency of Hg^{2+} progressively increased with an increase in the concentration of Tween 20-Au NPs increased and reached a saturation plateau at 33.2 nM (Figure 3B). Tween 20-Au NPs (33.2 nM) removed 99.85, 99.82, 99.80, 54.41, 21.18, and 18.61% of 10, 50, 100, 250, 750, and 100 μM Hg^{2+} in artificial seawater within 30 min, respectively (Figure S4, Supporting Information). We next investigated the effect of solution pH on the removal of Hg^{2+} with Tween 20-Au NPs. Figure 3C shows that the elimination efficiency of 10 μM Hg^{2+} with Tween 20-Au NPs (8.3 nM) remained above >99.7% in the pH range of 2.0 to 8.5, signifying that the sorption efficiency of Hg^{2+} onto the surface of Tween 20-Au NPs is independent of change pH between 2.0 and 8.5. This is attributed to the fact that Tween 20-Au NPs are stable in a wide pH range.[27−30] The reusability of Tween 20-Au NPs (8.3 nM) was evaluated when they were used to remove 10 μM Hg^{2+} from artificial seawater. Puntes et al. suggested that a thermal process can be used to recover gold from Au−Hg amalgam because the volatility of Hg^0 increases with temperature.[23] Note that the volatility of Hg^0 at 20 °C is 0.056 mg/h-cm^2. Thus, a mixture of Hg^{2+}-adsorbed gold NPs and reduced graphite oxide−Fe_3O_4 NP composites was heated at different temperatures for 10 min. Figure S5 (Supporting Information) shows that the optimal temperature for the regeneration of gold NPs was 80 °C. The elimination efficiency of Hg^{2+} was still larger than 95.0% after 10 repeated adsorption and desorption cycles. (Figure 3D). The elimination efficiency of Hg^{2+} remained more than 60% after recycling 15 times. This result clearly reflects that the developed nanomaterials were reusable for removing Hg^{2+} from artificial seawater.

The ability of Tween 20-Au NPs to trap Hg^{2+} was tested in the presence of other added metal ions. When Tween 20-Au NPs (8.3 nM) were incubated with a mixture of 10 μM Hg^{2+} and 10 μM Pb^{2+} in artificial seawater for 30 min, the elimination efficiency of Hg^{2+} remained above 99.3% (Figure 4A). Similar results were observed when Pb^{2+} was substituted by other metal ions, including Cr^{3+}, Cu^{2+}, Ag^{+}, Zn^{2+}, Cd^{2+}, Fe^{2+}, Fe^{3+}, and Al^{3+}. The adsorption capability of Tween 20-Au NPs was apparently maintained in the presence of possible interfering metal ions. A previous study reported that Tween

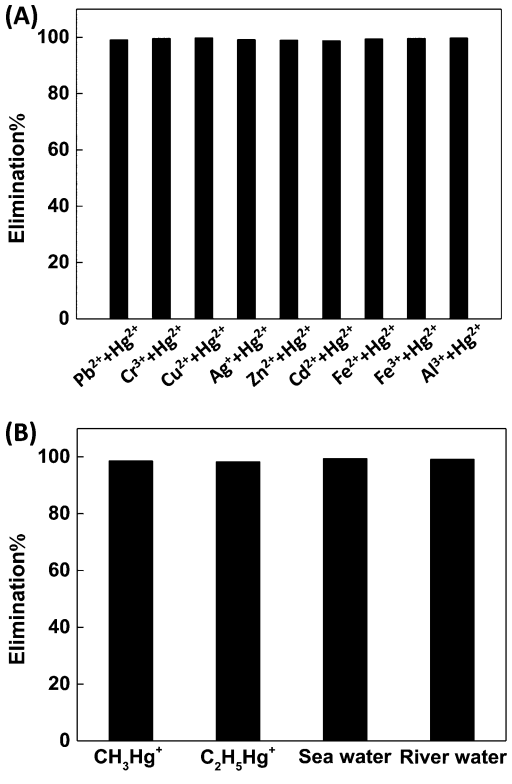

Figure 4. Effects of (A) possible interfered metal ions on the elimination efficiency of Hg^{2+} and (B) elimination efficiency of CH_3Hg^+(10 μM) in artificial seawater, $CH_2H_5Hg^+$ (10 μM) in artificial seawater, Hg^{2+}(15 μM) in river water, and Hg^{2+} (15 μM) in seawater by Tween 20-Au NPs. (A) A mixture of Hg^{2+} (10 μM) and added metal ions (10 μM) was incubated with 8.3 nM Tween 20-Au NPs in artificial seawater for 30 min. (B) Mercury species were incubated with 8.3 nM Tween 20-Au NPs for 30 min.

20-Au NPs were suited for sensing Hg^{2+} and Ag^+.[30] Tween 20-Au NPs were selective for Hg^{2+} in the presence of NaCl because NaCl served as a masking agent for Ag^+. When 10 μM Ag^+ was added to artificial seawater, the concentration of Ag^+ (K_{sp} of AgCl is 1.8×10^{-10}) was calculated to be 2.4 nM. Thus, we suggest that Ag^+ could not be adsorbed on the surface of Tween 20-Au NPs in artificial seawater. Furthermore, Tween 20-Au NPs efficiently (>99% elimination efficiency) removed other mercury species (CH_3Hg^+ and $C_2H_5Hg^+$) within 30 min, suggesting that they can provide a high affinity for organic mercury species (Figure 4B). Similarly, Chang et al. observed that citrate-capped gold NPs interacted strongly with organic mercury species.[24] However, thermal heating of CH_3Hg^+-adsorbed gold NPs is an ineffective means for CH_3Hg^+ recovery (Figure S6, Supporting Information). The selectivity of Tween 20-Au NPs toward Hg^{2+} was evaluated in river water and seawater. Tween 20-Au NPs (8.3 nM) removed >99.1% of the Hg^{2+} (1.2 mL, 15 μM) in river water and seawater (Figure 4B). This result strongly suggests that the proposed method is largely free from the matrix effect of river water and seawater.

To clarify the interaction between Hg^{2+} and Tween 20-Au NPs, we investigated the adsorption isotherm of Hg^{2+} on Tween 20-Au NPs. Figure S7 (Supporting Information) shows the adsorption capacity of Hg^{2+} progressively increased with an increase in the equilibrium concentration of Hg^{2+} and reached saturation. This could be attributed to the fact that an increase in the Hg^{2+} concentrations could accelerate the diffusion of Hg^{2+} on the surface of Tween 20-Au NPs. The equilibrium data were analyzed by the Langmuir and Freundlich isotherm models (Figures S8 and S9, Supporting Information). According to a comparison of the correlation coefficient (R^2) values, the Langmuir model (R^2 = 0.9815) fit the data better than the Freundlich model (R^2 = 0.6278), signifying that the adsorption of Hg^{2+} causes the formation of a monolayer on the surface of Tween 20-Au NPs. By applying the Langmuir model, the maximum adsorption capacity (q_{max}) of Hg^{2+} on Tween 20-Au NPs was estimated to be 47.6 mg/g. We compared the proposed model to the reported NP-based methods for removing Hg^{2+}, and we suggest that the distinct advantages of the proposed method are that it is simple, fast (within 30 min), durable (>10 cycles), and highly selective (Table S1, Supporting Information). More importantly, the proposed method can remove Hg^{2+} in a complex matrix and wide pH range.

Evidence of the Deposition of Hg^{2+} on the Surface of Tween 20-Au Nanoparticles. Previous studies have reported that deposition of Hg^{2+} on the surface of citrate-capped gold NPs resulted in a slight blue shift in surface plasmon resonance (SPR), an increase in particle size, and the presence of Hg in the XPS spectrum.[23,26] To determine whether or not Tween 20-Au NPs and citrate-capped gold NPs exhibited the same behavior for capturing Hg^{2+} in a high-salt matrix, we initially monitored the extinction spectra of Tween 20-Au NPs in the absence or presence of Hg^{2+}. The SPR wavelength of Tween 20-Au NPs was 523 nm (Curve a in Figure 5A). After adding 10 μM Hg^{2+}, the SPR wavelength of Tween 20-Au NPs shifted to 521 nm (Curve b in Figure 5A). This blue shift in the SPR band was characteristic of the presence of Hg^0 in Au NPs.[26] Figure 5B exhibits a comparison of the NPs before and after adding Hg^{2+}. The presence of Hg^0 in Au NPs caused an obvious increase in particle size.[26] This phenomenon arose from the well-known swelling effect as a result of the diffusion of Hg atoms into gold NPs. To determine whether Hg^{2+} was reduced to Hg^0, XPS was used to measure the content and valence states of Tween 20-Au NPs in the absence and presence of Hg^{2+}. The XPS spectrum of the dried Tween 20-Au NPs exhibited two peaks that corresponded to Au $4f_{5/2}$ at 87.5 eV and Au $4f_{7/2}$ at 83.8 eV (Curve a in Figure 5C). The line of best fit indicates that the Tween 20-Au NPs contained 2.7% Au^+ and 97.3% Au^0. After treating Tween 20-Au NPs with Hg^{2+}, the binding energies of the Au $4f_{5/2}$ and Au $4f_{7/2}$ electrons in the Tween 20-Au NPs were 87.6 and 83.9 eV, respectively, reflecting the presence of 3.1% Au^+ and 96.9% Au^0 in the Tween 20-Au NPs (Curve b in Figure 5C). Because the content of Au^0 in the Tween 20-Au NPs remained almost constant before and after the Hg^{2+} treatment, we reasoned that the reduction of Hg^{2+} to Hg^0 was not due to the difference in standard reduction potentials between Hg^{2+} and Au^0 ($2Au^0 + 3Hg^{2+} \rightarrow 2Au^{3+} + 3Hg^0$, emf = −0.5 V). Adding Hg^{2+} to the Tween 20-Au NP solution resulted in two weak binding-energy peaks at 99.2 and 103.4 eV, which were assigned to Hg $4f_{7/2}$ and Hg $4f_{5/2}$, respectively (Figure 5D). The binding energy of Hg $4f_{7/2}$ at 99.2 eV (Hg^0) indicated the appearance of Hg^0 in the Tween 20-Au NPs.[47] This finding confirms that citrate ions adsorbed on the surface of Tween 20-Au NPs can reduce Hg^{2+} to Hg^0. The deposition of Hg^{2+} on the surface of Tween 20-Au NPs was also detected using SEM equipped with EDX detectors. The EDS spectrum reveals the existence of Hg in the Tween 20- Au NPs after the treatment of Tween 20-Au NPs with Hg^{2+} (Figure S10, Supporting Information).

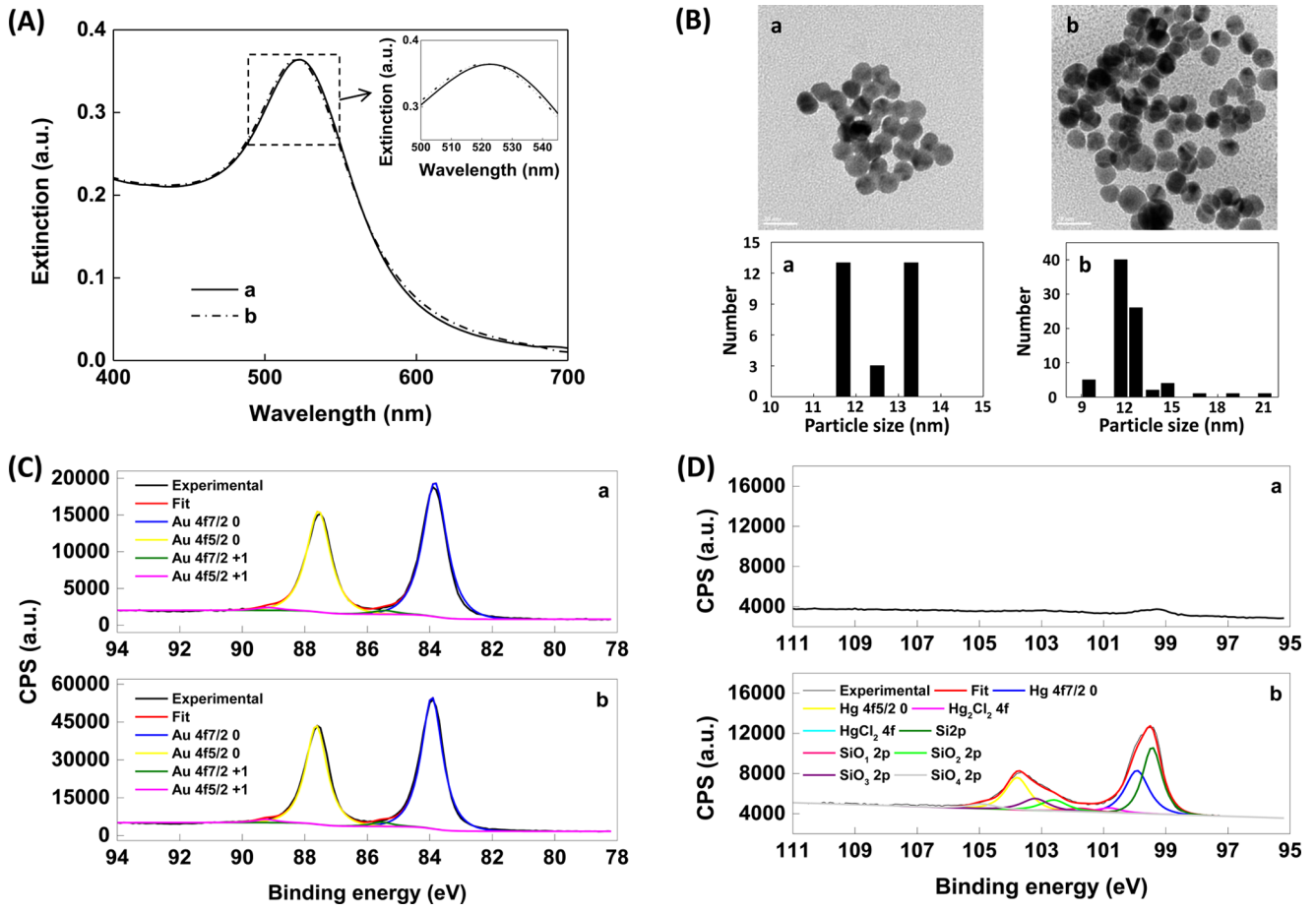

Figure 5. (A) Extinction spectra, (B) TEM images, (C) XPS spectra of Au 4f region, and (D) XPS spectra of Hg 4f region of 8.3 nM Tween 20-Au NPs (a) before and (b) after the addition of 10 μM Hg^{2+}.

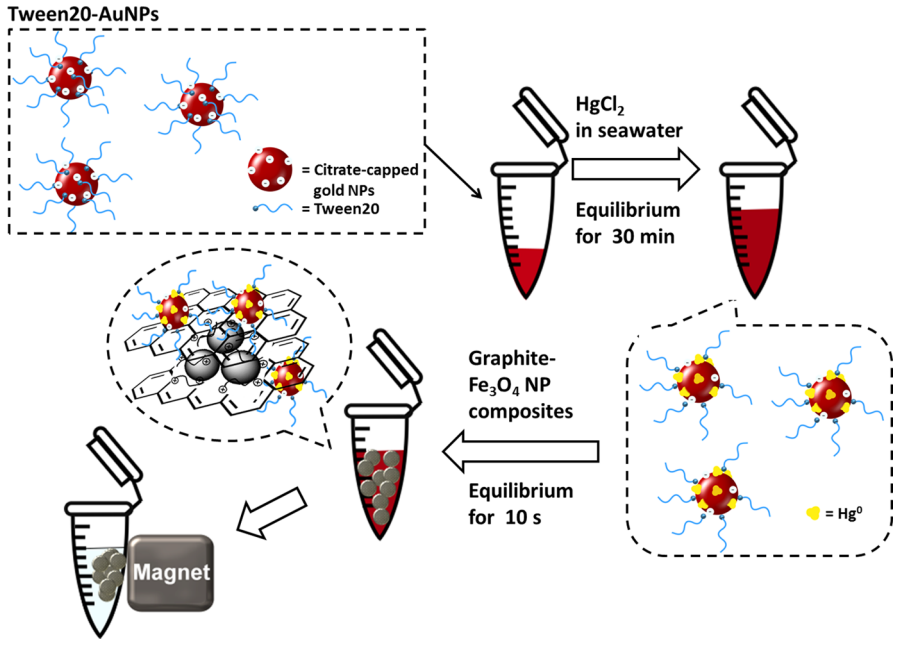

Figure 6. Procedure associated with the removal of Hg^{2+} by the combination of Tween 20-Au NPs and reduced graphite-Fe_3O_4 NP composites.

According to the aforementioned results, we outlined the procedure for removing Hg^{2+} via the combination of Tween 20-Au NPs and reduced graphite oxide−Fe_3O_4 NP composites (Figure 6). Tween 20-Au NPs are selective, efficient, and rapid to capture Hg^{2+} in high-salt matrices when gold NPs catalyze the citrate-ion-induced reduction of Hg^{2+} to Hg^0 on the NP surface. After Hg^0 is deposited onto the NP surface, Hg^0 diffuses into the Tween 20-Au NPs. By applying an external

dx.doi.org/10.1021/am5033988 | ACS Appl. Mater. Interfaces 2014, 6, 17437−17445

magnetic field, the Hg^0-containing gold NPs are collected using reduced graphite oxide−Fe_3O_4 NP composites. ICP-MS is used to quantify the concentration of Hg^{2+} in the supernatant and thus determine the elimination efficiency. Hg^0 in gold NPs evaporates under thermal treatment. The thermal-treated nanomaterials can be reused for removing Hg^{2+} from high-salt matrices. Video S1 (Supporting Information) shows the process for removing Hg^{2+} in seawater by using Tween 20-Au NPs as adsorbents and reduced graphite oxide−Fe_3O_4 NP composites as collectors of the Tween 20-Au NPs.

CONCLUSION

This study demonstrated that the combination of Tween 20-Au NPs and reduced graphite oxide−Fe_3O_4 NP composites facilitates the selective, efficient (>99% elimination efficiency), and rapid (within 30 min) removal of Hg^{2+}, CH_3Hg^+, and $C_2H_5Hg^+$ from artificial seawater, river water, and seawater. The procedure for eliminating Hg^{2+} involved the citrate ion-induced reduction of Hg^{2+} to Hg^0 on the NP surface and the collection of Hg^0-containing gold NPs by using reduced graphite oxide−Fe_3O_4 NP composites. When drinking water containing 5 μM Hg^{2+} was treated using the proposed method, the concentration of the remaining Hg^{2+} decreased to the maximal level (10 nM, 2 ppb) of mercury permissible in drinking water, as specified by the U.S. Environmental Protection Agency. This strategy can be modified to determine the levels of other heavy metal ions in an aqueous solution by replacing the Tween 20-Au NPs with other ligand-functionalized gold NPs. Previous studies have reported that 5-thiol-(2-nitrobenzoic acid)- and gallic acid-capped gold NPs were used to detect Cr^{3+} and Pb^{2+} through coordination between capping ligands and heavy metal ions.[48,49] Therefore, we suggest that reduced graphite oxide−Fe_3O_4 NP composites combined with either 5-thiol-(2-nitrobenzoic acid)-capped gold NPs or gallic acid-capped gold NPs could be useful for the removal of Cr^{3+} and Pb^{2+}, respectively, from aqueous solutions.

ASSOCIATED CONTENT

Supporting Information

The synthesis of citrate-capped gold NPs (Experimental Section); XPS spectra of reduced graphite oxide−Fe_3O_4 NP composites before and after the collection of Tween 20-Au NPs (Figure S1); extinction spectrum of citrate-capped gold NPs and Tween 20-Au NPs in artificial seawater (Figures S2 and S3); effect of the concentration of Hg^{2+} on the elimination efficiency (Figure S4); adsorption isotherms of Hg^{2+} by Tween 20-Au NPs (Figure S5); Langmuir and Freundlich adsorption isotherm plots of Tween 20-Au NPs in Hg^{2+} removal (Figure S6 and S7); SEM images and EDS spectrum of a mixture of Hg^{2+} and Tween 20-Au NPs (Figure S8); and comparison of other NP-based methods for the removal of Hg^{2+} (Table S1). This material is available free of charge via the Internet at http://pubs.acs.org.

AUTHOR INFORMATION

Corresponding Author

*E-mail: tsengwl@mail.nsysu.edu.tw. Fax: 011-886-7-3684046.

Notes

The authors declare no competing financial interest.

ACKNOWLEDGMENTS

We would like to thank the Ministry of Science and Technology (NSC 100-2628-M-110-001-MY4) for the financial support of this study.

REFERENCES

(1) Holmes, P.; James, K. A.; Levy, L. S. Is Low-Level Environmental Mercury Exposure of Concern to Human Health? *Sci. Total Environ.* **2009**, *408*, 171−182.
(2) Wood, C. M.; McDonald, M. D.; Walker, P.; Grosell, M.; Barimo, J. F.; Playle, R. C.; Walsh, P. J. Bioavailability of Silver and Its Relationship to Ionoregulation and Silver Speciation Across a Range of Salinities in the Gulf Toadfish (*Opsanus beta*). *Aquat. Toxicol.* **2004**, *70*, 137−57.
(3) Boening, D. W. Ecological Effects, Transport, and Fate of Mercury: A General Review. *Chemosphere* **2000**, *40*, 1335−51.
(4) Biester, H.; Schuhmacher, P.; Muller, G. Effectiveness of Mossy Tin Filters to Remove Mercury from Aqueous Solution by Hg(0) Reduction and Hg(0) Amalgamation. *Water Res.* **2000**, *34*, 2031−2036.
(5) Huttenloch, P.; Roehl, K. E.; Czurda, K. Use of Copper Shavings to Remove Mercury from Contaminated Groundwater or Wastewater by Amalgamation. *Environ. Sci. Technol.* **2003**, *37*, 4269−4273.
(6) Chojnacki, A.; Chojnacka, K.; Hoffmann, J.; Gorecki, H. The Application of Natural Zeolites for Mercury Removal: From Laboratory Tests to Industrial Scale. *Miner. Eng.* **2004**, *17*, 933−937.
(7) Oehmen, A.; Viegas, R.; Velizarov, S.; Reis, M. A. M.; Crespo, J. G. Removal of Heavy Metals from Drinking Water Supplies through the Ion Exchange Membrane Bioreactor. *Desalination* **2006**, *199*, 405−407.
(8) Zhang, H. Photochemical Redox Reactions of Mercury. *Struct. Bonding (Berlin, Ger.)* **2006**, *120*, 37−79.
(9) Chakrabarty, K.; Saha, P.; Ghoshal, A. K. Separation of Mercury from Its Aqueous Solution through Supported Liquid Membrane Using Environmentally Benign Diluent. *J. Membr. Sci.* **2010**, *350*, 395−401.
(10) Mahmoud, M. E.; Osman, M. M.; Amer, M. E. Selective Pre-Concentration and Solid Phase Extraction of Mercury(II) from Natural Water by Silica Gel-Loaded Dithizone Phases. *Anal. Chim. Acta* **2000**, *415*, 33−40.
(11) Evangelista, S. M.; DeOliveira, E.; Castro, G. R.; Zara, L. F.; Prado, A. G. S. Hexagonal Mesoporous Silica Modified with 2-Mercaptothiazoline for Removing Mercury from Water Solution. *Surf. Sci.* **2007**, *601*, 2194−2202.
(12) Soliman, E. M.; Saleh, M. B.; Ahmed, S. A. Alumina Modified by Dimethyl Sulfoxide as a New Selective Solid Phase Extractor for Separation and Preconcentration of Inorganic Mercury(II). *Talanta* **2006**, *69*, 55−60.
(13) Ahmed, S. A. Alumina Physically Loaded by Thiosemicarbazide for Selective Preconcentration of Mercury(II) Ion from Natural Water Samples. *J. Hazard. Mater.* **2008**, *156*, 521−529.
(14) Pourreza, N.; Ghanemi, K. Determination of Mercury in Water and Fish Samples by Cold Vapor Atomic Absorption Spectrometry after Solid Phase Extraction on Agar Modified with 2-Mercaptobenzimidazole. *J. Hazard. Mater.* **2009**, *161*, 982−987.
(15) Park, H. G.; Kim, T. W.; Chae, M. Y.; Yoo, I. K. Activated Carbon-Containing Alginate Adsorbent for the Simultaneous Removal of Heavy Metals and Toxic Organics. *Process Biochem.* **2007**, *42*, 1371−1377.
(16) Li, X. G.; Feng, H.; Huang, M. R. Strong Adsorbability of Mercury Ions on Aniline/Sulfoanisidine Copolymer Nanosorbents. *Chem.—Eur. J.* **2009**, *15*, 4573−4581.
(17) Ralston, N. Nanomaterials: Nano-Selenium Captures Mercury. *Nat. Nanotechnol.* **2008**, *3*, 527−528.
(18) Lisha, K. P.; Maliyekkal, S. M.; Pradeep, T. Manganese Dioxide Nanowhiskers: A Potential Adsorbent for the Removal of Hg(II) from Water. *Chem. Eng. J.* **2010**, *160*, 432−439.

(19) Luo, G. Q.; Yao, H.; Xu, M. H.; Cui, X. W.; Chen, W. X.; Gupta, R.; Xu, Z. H. Carbon Nanotube-Silver Composite for Mercury Capture and Analysis. *Energy Fuel.* **2010**, *24*, 419−426.
(20) Sumesh, E.; Bootharaju, M. S.; Anshup; Pradeep, T. A Practical Silver Nanoparticle-Based Adsorbent for the Removal of Hg^{2+} from Water. *J. Hazard. Mater.* **2011**, *189*, 450−457.
(21) Yordanova, T.; Vasileva, P.; Karadjova, I.; Nihtianova, D. Submicron Silica Spheres Decorated with Silver Nanoparticles as a New Effective Sorbent for Inorganic Mercury in Surface Waters. *Analyst* **2014**, *139*, 1532−1540.
(22) Lisha, K. P.; Anshup; Pradeep, T. Towards a Practical Solution for Removing Inorganic Mercury from Drinking Water Using Gold Nanoparticles. *Gold Bull.* **2009**, *42*, 144−152.
(23) Ojea-Jimenez, I.; Lopez, X.; Arbiol, J.; Puntes, V. Citrate-Coated Gold Nanoparticles As Smart Scavengers for Mercury(II) Removal from Polluted Waters. *ACS Nano* **2012**, *6*, 2253−2260.
(24) Lo, S. I.; Chen, P. C.; Huang, C. C.; Chang, H. T. Gold Nanoparticle-Aluminum Oxide Adsorbent for Efficient Removal of Mercury Species from Natural Waters. *Environ. Sci. Technol.* **2012**, *46*, 2724−2730.
(25) Lee, Y. F.; Nan, F. H.; Chen, M. J.; Wu, H. Y.; Ho, C. W.; Chen, Y. Y.; Huang, C. C. Detection and Removal of Mercury and Lead Ions by Using Gold Nanoparticle-Based Gel Membrane. *Anal. Methods* **2012**, *4*, 1709−1717.
(26) Mertens, S. F. L.; Gara, M.; Sologubenko, A. S.; Mayer, J.; Szidat, S.; Kramer, K. W.; Jacob, T.; Schiffrin, D. J.; Wandlowski, T. Au@Hg Nanoalloy Formation Through Direct Amalgamation: Structural, Spectroscopic, and Computational Evidence for Slow Nanoscale Diffusion. *Adv. Funct. Mater.* **2011**, *21*, 3259−3267.
(27) Chang, C. W.; Tseng, W. L. Gold Nanoparticle Extraction Followed by Capillary Electrophoresis to Determine the Total, Free, and Protein-Bound Aminothiols in Plasma. *Anal. Chem.* **2010**, *82*, 2696−2702.
(28) Shen, C. C.; Tseng, W. L.; Hsieh, M. M. Selective Enrichment of Aminothiols Using Polysorbate 20-Capped Gold Nanoparticles Followed by Capillary Electrophoresis with Laser-Induced Fluorescence. *J. Chromatogr A* **2009**, *1216*, 288−93.
(29) Zhao, Y. Y.; Wang, Z.; Zhang, W.; Jiang, X. Y. Adsorbed Tween 80 Is Unique in Its Ability to Improve the Stability of Gold Nanoparticles in Solutions of Biomolecules. *Nanoscale* **2010**, *2*, 2114−2119.
(30) Lin, C. Y.; Yu, C. J.; Lin, Y. H.; Tseng, W. L. Colorimetric Sensing of Silver(I) and Mercury(II) Ions Based on an Assembly of Tween 20-Stabilized Gold Nanoparticles. *Anal. Chem.* **2010**, *82*, 6830−6837.
(31) Lin, J. H.; Chang, C. W.; Wu, Z. H.; Tseng, W. L. Colorimetric Assay for *S*-Adenosylhomocysteine Hydrolase Activity and Inhibition Using Fluorosurfactant-Capped Gold Nanoparticles. *Anal. Chem.* **2010**, *82*, 8775−8779.
(32) Lin, J. H.; Chang, C. W.; Tseng, W. L. Fluorescent Sensing of Homocysteine in Urine: Using Fluorosurfactant-Capped Gold Nanoparticles and *o*-Phthaldialdehyde. *Analyst* **2010**, *135*, 104−110.
(33) Lu, C.; Zu, Y.; Yam, V. W. Specific Postcolumn Detection Method for HPLC Assay of Homocysteine Based on Aggregation of Fluorosurfactant-Capped Gold Nanoparticles. *Anal. Chem.* **2007**, *79*, 666−672.
(34) Fujimoto, T.; Miya, M.; Machida, M.; Takechi, S.; Kakinoki, S.; Kanda, K.; Nomura, A. Improved Recovery of Human Urinary Protein for Electrophoresis. *J. Health Sci.* **2006**, *52*, 718−723.
(35) Wu, Z. H.; Tseng, W. L. Combined Cloud Point Extraction and Tween 20-Stabilized Gold Nanoparticles for Colorimetric Assay of Silver Nanoparticles in Environmental Water. *Anal. Methods* **2011**, *3*, 2915−2920.
(36) Hummers, W. S.; Offeman, R. E. Preparation of Graphitic Oxide. *J. Am. Chem. Soc.* **1958**, *80*, 1339−1339.
(37) Bradder, P.; Ling, S. K.; Wang, S. B.; Liu, S. M. Dye Adsorption on Layered Graphite Oxide. *J. Chem. Eng. Data* **2011**, *56*, 138−141.
(38) Kim, F.; Luo, J. Y.; Cruz-Silva, R.; Cote, L. J.; Sohn, K.; Huang, J. X. Self-Propagating Domino-like Reactions in Oxidized Graphite. *Adv. Funct. Mater.* **2010**, *20*, 2867−2873.
(39) Ji, Z. Y.; Zhu, G. X.; Shen, X. P.; Zhou, H.; Wu, C. M.; Wang, M. Reduced Graphene Oxide Supported FePt Alloy Nanoparticles with High Electrocatalytic Performance for Methanol Oxidation. *New J. Chem.* **2012**, *36*, 1774−1780.
(40) Jeong, H. K.; Lee, Y. P.; Lahaye, R. J.; Park, M. H.; An, K. H.; Kim, I. J.; Yang, C. W.; Park, C. Y.; Ruoff, R. S.; Lee, Y. H. Evidence of Graphitic AB Stacking Order of Graphite Oxides. *J. Am. Chem. Soc.* **2008**, *130*, 1362−1366.
(41) Jeong, H. K.; Colakerol, L.; Jin, M. H.; Glans, P. A.; Smith, K. E.; Lee, Y. H. Unoccupied Electronic States in Graphite Oxides. *Chem. Phys. Lett.* **2008**, *460*, 499−502.
(42) Guo, Y. Q.; Bao, C. L.; Song, L.; Yuan, B. H.; Hu, Y. In Situ Polymerization of Graphene, Graphite Oxide, and Functionalized Graphite Oxide into Epoxy Resin and Comparison Study of On-the-Flame Behavior. *Ind. Eng. Chem. Res.* **2011**, *50*, 7772−7783.
(43) Zhang, S.; Shao, Y. Y.; Liao, H. G.; Engelhard, M. H.; Yin, G. P.; Lin, Y. H. Polyelectrolyte-Induced Reduction of Exfoliated Graphite Oxide: A Facile Route to Synthesis of Soluble Graphene Nanosheets. *ACS Nano* **2011**, *5*, 1785−1791.
(44) Ma, Z. Y.; Guan, Y. P.; Liu, H. Z. Synthesis and Characterization of Micron-Sized Monodisperse Superparamagnetic Polymer Particles with Amino Groups. *J. Polym. Sci., Part A: Polym. Chem.* **2005**, *43*, 3433−3439.
(45) Jeon, K. J.; Lee, Z. Size-Dependent Interaction of Au Nanoparticles and Graphene Sheet. *Chem. Commun.* **2011**, *47*, 3610−3612.
(46) Dave, N.; Chan, M. Y.; Huang, P. J. J.; Smith, B. D.; Liu, J. W. Regenerable DNA-Functionalized Hydrogels for Ultrasensitive, Instrument-Free Mercury(II) Detection and Removal in Water. *J. Am. Chem. Soc.* **2010**, *132*, 12668−12673.
(47) Genin, F.; Alnot, M.; Ehrhardt, J. J. Interaction of Vapours of Mercury with PbS(001): A Study by X-ray Photoelectron Spectroscopy, RHEED and X-ray Absorption Spectroscopy. *Appl. Surf. Sci.* **2001**, *173*, 44−53.
(48) Huang, K. W.; Yu, C. J.; Tseng, W. L. Sensitivity Enhancement in the Colorimetric Detection of Lead(II) Ion Using Gallic Acid-Capped Gold Nanoparticles: Improving Size Distribution and Minimizing Interparticle Repulsion. *Biosens. Bioelectron.* **2010**, *25*, 984−989.
(49) Lai, Y. J.; Tseng, W. L. Role of 5-Thio-(2-nitrobenzoic acid)-Capped Gold Nanoparticles in the Sensing of Chromium(VI): Remover and Sensor. *Analyst* **2011**, *136*, 2712−2717.